Top and Bottom Gate Oxide Thicknesses Dependent Subthreshold Swing in Asymmetric Junctionless Double Gate MOSFET

Hakkee Jung
Department of Electronic Engineering, Kunsan National University, Gunsan, Republic of Korea
Email: hkjung@kunsan.ac.kr

Abstract—**We investigate the dependence of the Subthreshold Swing (*SS*) of asymmetric junctionless double gate MOSFETs on the top gate oxide thickness t_{ox1} and the bottom gate oxide thickness t_{ox2}. The Poisson equation is used to derive the channel potential distribution of the transistor to the analytical series form, and the analytical subthreshold swing is obtained using series type potential distribution. This model is found to be in good agreement with the 2D simulation. In the asymmetric structure, since the gate oxide thicknesses at the top and bottom sides can be made different, the oxide film thickness dependency can be compared with that of the symmetric structure which has identical top and bottom gate oxide film thicknesses. As a result, we observes that the geometric mean of the top and bottom gate oxide thicknesses is linearly proportional to the subthreshold swing. In other words, we derive the relationship of $SS = K\sqrt{t_{ox1}t_{ox2}}$, and observe that the proportional constant *K* changes with channel length and channel thickness. It is found that as the channel length decreases and the channel thickness increases, it increases sharply. It is also found that the *K* changes with more sensitivity to channel thickness than to channel length.**

Index Terms—**asymmetric, geometric mean, junctionless, subthreshold swing, oxide thickness**

I. Introduction

The desire for a transistor structure to reduce the short channel effect has led to the development of multi-gate transistors, and the multi-gate structure has been adapted into various structures such as the double gate structure, the Fin structure, and the cylindrical structure [1]-[6]. The simplest structure is the double gate structure and this study will focus on the double gate MOSFET structure. Especially, the junctionless structure was developed for when the channel is shorter because the junction-based structure shows a limitations for rapid doping type and concentration change between the source/drain and the channel [7], [8]. In the junctionless structure, not only the doping type between the source/drain and the channel but also the doping concentration are made consistent so that the process difficulties that arise in short channel junction-based MOSFETs can be overcome. The development of such a structure is intended to overcome the severe device performance degradation in short channels.

The junction-based Double Gate (DG) MOSFET structure has been investigated with symmetric top and bottom gates, and many studies have also been conducted on the asymmetric structure in the junction-based MOSFET [9]-[12]. But there is little research on asymmetric junctionless DGMOSFETs. The asymmetric and junctionless structures are very important for implementing the short channel devices because the two structures can reduce the short channel effects which include degradation of Subthreshold Swing (SS) and threshold voltage roll-off, as well as drain induced barrier lowering. Therefore, in this study, we will investigate the influence of the change in top and bottom gate oxide thicknesses on the subthreshold swing of the junctionless DGMOSFET with an asymmetric structure.

In the asymmetric structure, it is advantageous to fabricate different thicknesses for the top and bottom oxide films. Therefore, it is possible to more effectively reduce the short channel effect because the number of elements that can control the short channel effect increases. Jiang *et al*. have studied the short-channel effect only for symmetric junctionless DGMOSFETs, and Ding *et al*. proposed a subthreshold swing model of both the symmetric and asymmetric junction-based DGMOSFET using series type potential distribution [13], [14]. In this study, we will present a subthreshold swing model for the asymmetric junctionless DGMOSFET by modifying the Ding's potential and subthreshold swing models. Ding *et al.* reported that the bottom gate oxide thickness of a junction-based DGMOSFET operating in an inversion model has little effect on the subthreshold swing. The reason is that the center of conduction shifts to the top gate with decreasing of top gate oxide film thickness and the top gate voltage can better control the charges in the channel of junction-based DGMOSFETs if the top gate oxide thickness is reduced. However, in the case of a junctionless MOSFET operating in accumulation mode, the influence of top and bottom gate oxide thicknesses on the subthreshold swing will have a different relationship with the junction-based

Manuscript received October 5, 2018; revised December 26, 2018; accepted December 26, 2018.
Corresponding author: Hakkee Jung (email: hkjung@kunsan.ac.kr).

©2019 Int. J. Elec. & Elecn. Eng. & Telcomm.

doi: 10.18178/ijeetc.8.5.292-296

DGMOSFET because the center of conduction is always centered between the top gate and the bottom gate. We will analyze the subthreshold swing according to the change of top and bottom gate oxide thicknesses using the modified model. For this purpose, the potential model of the series type is derived from the Poisson equation, and the top and bottom gate oxide thicknesses are used as variables.

This paper is arranged as follows: the analytical subthreshold swing is described in Section II; we present the effects of the top and bottom gate oxide thicknesses on subthreshold swing and discuss the results in Section III; and we conclude in Section IV.

II. Analytical Subthreshold Swing Model of the Asymmetric Junctionless DGMOSFET

Fig. 1 shows a schematic diagram of the asymmetric junctionless DGMOSFET used in this paper. The source and the drain were doped with a high concentration and the channel was doped with N_d=10^{19} per cm^3. The top and bottom gate voltages are V_{gt} and V_{gb}, respectively. The L_g is the gate length, the t_{si} channel thickness, and t_{ox1} and t_{ox2} the thicknesses of the oxide film at the top and bottom, respectively. The following Poisson equation is used to derive the potential distribution in the channel.

$$\partial^2\phi(x,y)/\partial x^2+\partial^2\phi(x,y)/\partial y^2=-N_d/\varepsilon_{si} \quad (1)$$

In this case, we use the following boundary conditions:

$$\phi(0,y)=V_s$$
$$\phi(L_g,y)=V_s+V_d$$
$$\phi(x,0)=V_{gt}-V_{fbt}+\frac{\varepsilon_{si}}{C_{ox1}}\left.\frac{\partial\phi}{\partial y}\right|_{y=0}$$
$$\phi(x,t_{si})=V_{gb}-V_{fbt}+\frac{\varepsilon_{si}}{C_{ox2}}\left.\frac{\partial\phi}{\partial y}\right|_{y=t_{si}},$$

where ε_{si} is the dielectric constant of silicon, V_{fbt} is the flat band voltage of the top gate, and V_{fbb} is the flat band voltage of the bottom gate. The potential distribution derived from the boundary conditions can be expressed as the follows using the Ding's expansion method [14]:

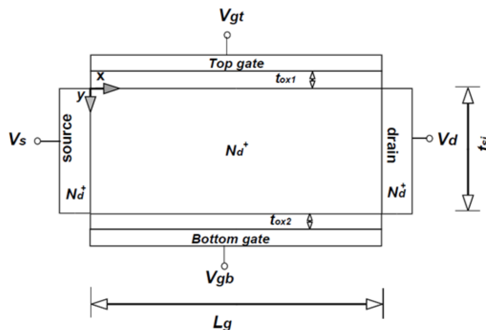

Fig. 1. Schematic cross sectional diagram of an asymmetric junctionless double gate MOSFET.

$$\phi(x,y)=V_s+\frac{V_d x}{L_g}+\sum_{n=1}^{\infty}A_n(y)\sin\frac{n\pi x}{L_g} \quad (2)$$

where

$$A_n(y)=C_n e^{k_n y}+D_n e^{-k_n y}-f_n/k_n$$

$$f_n=\begin{cases}-\dfrac{4qN_d}{n\pi\varepsilon_{si}}, & n=1,3,5,\cdots\\ 0, & n=2,4,6,\cdots\end{cases}$$

$$C_n=\frac{C_{ox1}\left[\begin{array}{c}(\varepsilon_{si}k_n-C_{ox2})(f_n-G_nk_n^2)+\\ r(C_{ox1}+\varepsilon_{si}k_n)(f_n-H_nk_n^2)e^{k_nt_{si}}\end{array}\right]}{k_n^2\left[\begin{array}{c}C_{ox1}\varepsilon_{si}k_n(1+r)(1+e^{2k_nt_{si}})-\\ (C_{ox1}C_{ox2}+\varepsilon_{si}^2k_n^2)(1-e^{2k_nt_{si}})\end{array}\right]}$$

$$D_n=\frac{C_{ox1}e^{k_nt_{si}}\left[\begin{array}{c}(\varepsilon_{si}k_n+C_{ox2})(f_n-G_nk_n^2)e^{k_nt_{si}}-\\ r(C_{ox1}-\varepsilon_{si}k_n)(f_n-H_nk_n^2)\end{array}\right]}{k_n^2\left[\begin{array}{c}C_{ox1}\varepsilon_{si}k_n(1+r)(1+e^{2k_nt_{si}})-\\ (C_{ox1}C_{ox2}+\varepsilon_{si}^2k_n^2)(1-e^{2k_nt_{si}})\end{array}\right]}$$

$$G_n=\begin{cases}\left(\dfrac{2}{n\pi}\right)\left[2(V_s-V_{gt}+V_{fbt})+V_d\right], & n=1,3,5,\cdots\\ 0, & n=2,4,6,\cdots\end{cases}$$

$$H_n=\begin{cases}\left(\dfrac{2}{n\pi}\right)\left[2(V_s-V_{gb}+V_{fbb})+V_d\right], & n=1,3,5,\cdots\\ 0, & n=2,4,6,\cdots\end{cases}$$

$$C_{ox1}=\varepsilon_{ox1}/t_{ox1},\quad C_{ox2}=\varepsilon_{ox2}/t_{ox2}$$
$$r=C_{ox2}/C_{ox1},\quad k_n=n\pi/L_g.$$

We use $\varepsilon_{ox1}=\varepsilon_{ox2}$ for silicon dioxide.

In the asymmetric structure, the subthreshold swing indicates the change in the top gate voltage with respect to the drain current change in the subthreshold region. If the electron density constituting the drain current can be approximated by a Boltzmann distribution such as $n\approx N_d e^{q\phi_{min}/kT}$, the following (3) can represent the subthreshold swing:

$$SS=\frac{\partial V_{gt}}{\partial\log I_{ds}}=\ln(10)\left(\frac{kT}{q}\right)\left(\frac{\partial\phi_{\min}}{\partial V_{gt}}\right)^{-1} \quad (3)$$

In this case, to obtain $\phi_{\min}$, x=$x_{\min}$ satisfying $\partial\phi(x,t_{si}/2)/\partial x=0$ is required, and then $\phi_{\min}$ can be obtained by substituting the $x_{\min}$ into (2). The majority carriers in the junctionless DGMOSFET will conduct current through the silicon body in the subthreshold region, whereas the induced minority carriers in the junction-based DGMOSFET flow at the region between the gate oxide and silicon body [15]. Therefore, the most of the electrons move through the center of the channel, so y=$t_{si}/2$ is used for the junctionless DGMOSFET. Consequently, the subthreshold swing can be expressed by

$$SS=\ln(10)\left(\frac{kT}{q}\right)\left[\sum_{n=1}^{\infty}\frac{4}{n\pi}\sin\left(\frac{n\pi x_{min}}{L_g}\right)\times\right.$$

©2019 Int. J. Elec. & Elecn. Eng. & Telcomm.

$$\left. \frac{C_{ox1}\left[e^{k_n t_{si}/2}\left(\varepsilon_{si}k_n - C_{ox2}\right) + e^{k_n t_{si}/2}\left(\varepsilon_{si}k_n - C_{ox2}\right)\right]}{C_{ox1}\varepsilon_{si}k_n\left(1+\dfrac{t_{ox1}}{t_{ox2}}\right)\left(1+e^{2k_n t_{si}}\right) - (C_{ox1}C_{ox2}+\varepsilon_{si}^2 k_n^2)\left(1+e^{2k_n t_{si}}\right)} \right]^{-1} \quad (4)$$

where k is the Boltzmann constant and T is the absolute temperature. Although the number of summation terms in (4) is infinite, we only use n=30 instead of infinite because A_n converges fastly for n [14]. When we inspect (4), it can be seen that the subthreshold swing changes according to the thickness of the top and bottom oxide films through the variables such as C_{ox1}, C_{ox2}, t_{ox1}, and t_{ox2}. In this paper, we compare the subthreshold swings in the symmetric junctionless DGMOSFET of $t_{ox1}=t_{ox2}$ with those of the asymmetric structure. In the case of an asymmetric junctionless DGMOSFET, we will show it is possible to further reduce the subthreshold swing by adjusting the thickness of the top and bottom oxide films. The gate and flat band voltages for the top and bottom gate sides can be also used differently, in the case of an asymmetric junctionless DGMOSFET which can fabricate differently the top and bottom gate oxide thicknesses. However, in order to observe only the effect of the top and bottom gate oxide thicknesses, we use the same values for the top and bottom gate voltages and the flat band voltages of top and bottom sides.

III. Subthreshold Swing for the Top and Bottom Gate Oxide Thicknesses

In order to verify the validity of (4), the two-dimensional simulation values and the results of (4) are compared in Fig. 2. As shown in Fig. 2, the two-dimensional simulation value and the values derived from the analytical subthreshold swing of (4) proposed in this paper are in good agreement for the range of channel length from 20 nm to 60 nm. Therefore, we will analyze the subthreshold swing of an asymmetric junctionless DGMOSFETs for different top and bottom oxide film thicknesses by using (4).

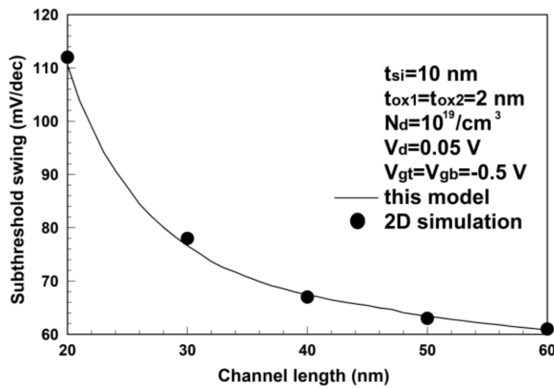

Fig. 2. Comparison of subthreshold swings against channel length using the analytical model and two dimensional simulation [13] under the given conditions.

Unlike the symmetrical structure, the asymmetric structure has an advantage that the oxide film thicknesses at the top and bottom sides can be fabricated with different thickness. The contours of the subthreshold swing is shown in Fig. 3 at channel lengths of 20 nm and 60 nm when the top gate oxide thickness and the bottom gate oxide thickness are changed from 1 nm to 5 nm in (4). The values not shown in the figure are the same as those used in Fig. 2, and the dashed line in Fig. 3 is the symmetrical case in which the top and bottom gate oxide thicknesses are the same. As shown in Fig. 3 (b), when the channel length increases to 60 nm, the subthreshold swing for the top and bottom gate oxide thicknesses hardly changes: it lies between 60-66 mV/dec for the oxide thickness range used in the calculation. However, if the channel length decreases to 20 nm, the subthreshold swing will vary greatly from 90 to 160 mV/dec. It can be seen that the symmetric structure has a single value but the asymmetric structure shows varied values depending on the thickness of the top and bottom gate oxide films. Fig. 3 shows that the subthreshold swings are kept constant when the top gate oxide thickness decreases and the bottom gate oxide thickness increases, and vice versa.

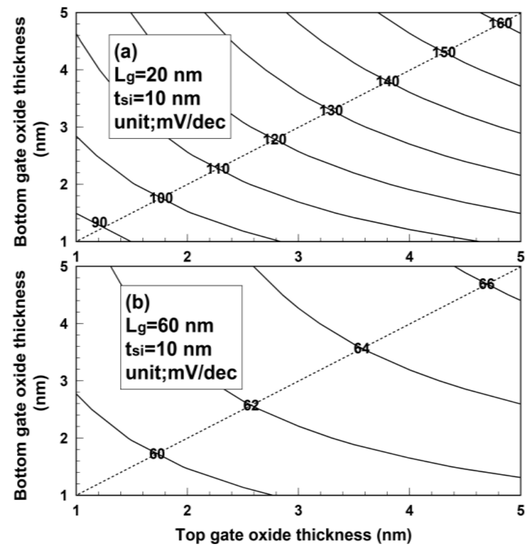

Fig. 3. Contours of subthreshold swings for top and bottom gate oxide thicknesses for given conditions at (a) L_g=20 nm and (b) L_g=60 nm.

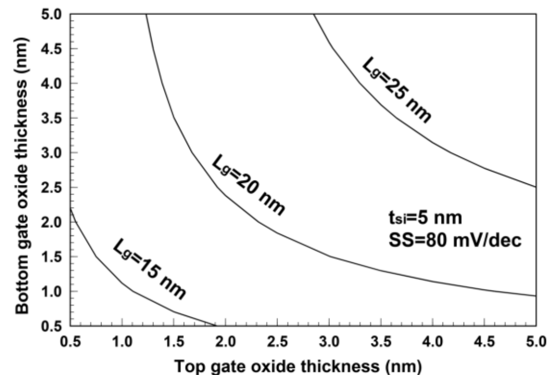

Fig. 4. Contours of subthreshold swings of 80 mV/dec for top and bottom gate oxide thicknesses for given conditions with a parameter of the channel length.

Fig. 4 shows the contour plot of subthreshold swing at 80 mV/dec with the channel length as a parameter. As shown in Fig. 4, if the channel length is reduced to about 15 nm, the thicknesses of the top and bottom oxide films

©2019 Int. J. Elec. & Elecn. Eng. & Telcomm.

must be reduced to about 1 nm for the symmetric structure in order to maintain a subthreshold swing of *SS*=80 mV/dec or less. However, if the channel length increases to 25 nm, film thickness may increase to 3.5 nm for the symmetric structure to maintain subthreshold swing of 80 mV/dec. In the case of an asymmetric junctionless DGMOSFET with channel length of 25 nm, it can be seen that nearly all the top and bottom oxide film thicknesses in the range are possible to maintain a subthreshold swing of *SS*=80 mV/dec or less. When the channel length is 15 nm in Fig. 4, it can be seen that the range of the top and bottom gate oxide thicknesses is very narrow to maintain a subthreshold swing of 80 mV/dec or less. However, when one of the top and bottom gate oxide films is made thinner, the other can become thicker. That is, when the oxide thickness of one gate is reduced to 0.5 nm, it may be observed that the subthreshold swing can be maintained at 80 mV/dec if the other gate oxide films is increased to a thickness of about 2 nm.

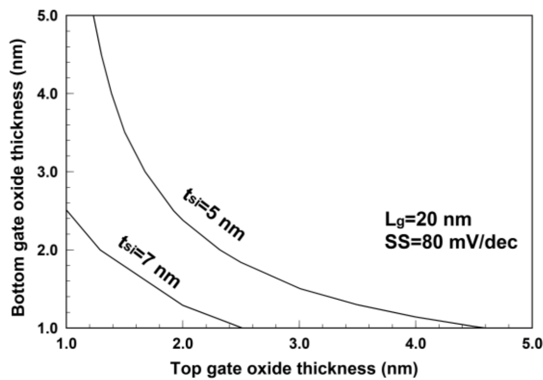

Fig. 5. Contours of subthreshold swings of 80 mV/dec for top and bottom gate oxide thicknesses for given conditions with a parameter of channel thickness.

The channel thickness and the channel length are also the important parameters in the short channel asymmetric junctionless DGMOSFET. Therefore, the contour graph of the subthreshold swing of 80 mV/dec for different top and bottom gate oxide film thicknesses is shown with channel thickness as a parameter in Fig. 5. As shown in Fig. 5, as the channel thickness decreases, the top and bottom gate oxide thicknesses should increase to maintain a subthreshold swing of 80 mV/dec. That is, when the channel thickness is reduced, the margin for the top and bottom gate oxide film thicknesses is increased to keep the subthreshold swing low. However, when the channel thickness is increased to 7 nm, to keep the subthreshold swing below 80 mV/dec the range of possible thicknesses of the top and bottom oxide films is very small. Comparing Fig. 5 with Fig. 4, note that subthreshold swing is more sensitive to deviation in channel thickness than to channel length.

Fig. 3, Fig. 4 and Fig. 5 show that there is a correlation between the top and bottom gate oxide thicknesses in order to keep the subthreshold swing constant. This relationship is the same as that observed when the scale length is proportional to the geometric mean of the channel thickness and the oxide thickness [16], so in this paper we analyzed the subthreshold swing for the geometric mean of the top and bottom gate oxide thicknesses.

Fig. 6 shows the relationship between the geometric mean of the top and bottom oxide thicknesses and the subthreshold swing with the channel length as a parameter. The results are shown as triangles, and the results of a linear fitting of the data are shown as the straight lines. As described above, it can be obtained that the geometric mean of the top and bottom oxide film thickness is linearly proportional to the subthreshold swing as the followings:

$$SS = K\sqrt{t_{ox1}t_{ox2}} \tag{5}$$

It can be seen that the proportional constant *K* increases sharply with decreasing channel length. When the channel length is increased to 60 nm or more, the subthreshold swing is independent of the thickness of the top and bottom oxide films, and kept nearly constant. However, as the channel length decreases, the subthreshold swing is observed to be sensitive to the geometric mean of the top and bottom oxide thicknesses due to the rapid increase of the proportional constant *K*.

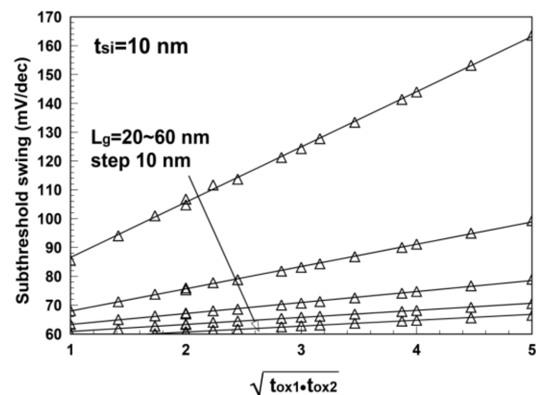

Fig. 6. Subthreshold swings for the geometric mean of top and bottom gate oxide thicknesses for given conditions with a parameter of channel length.

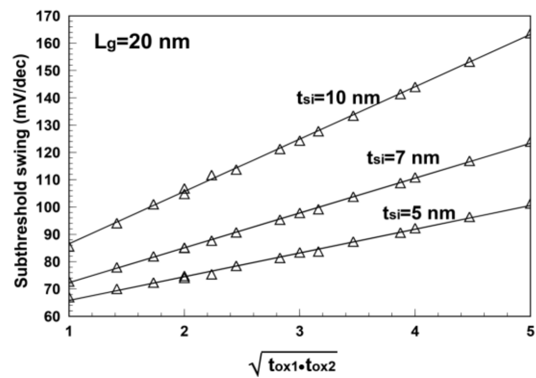

Fig. 7. Subthreshold swings for geometric mean of top and bottom gate oxide thicknesses for given conditions with a parameter of channel thickness

Fig. 7 shows the relationship between the geometric mean of the top and bottom oxide thicknesses and the subthreshold swing when the channel thickness is a parameter. It can be seen that as the channel thickness increases, the proportional constant *K* increases in (5). That is, as the channel thickness increases, the change in

©2019 Int. J. Elec. & Elecn. Eng. & Telcomm.

the subthreshold swing with respect to the change in the top and bottom oxide film thicknesses becomes more sensitive. As can be seen from the comparison of Fig. 6 and Fig. 7, the subthreshold swing is more sensitive to the change of the channel thickness than the channel length. As shown in Fig. 7, as the channel thickness decreases, the change of the subthreshold swing with respect to the geometric mean of the top and bottom oxide film thicknesses decreases. Therefore, it can be seen that as the channel length increases and the channel thickness decreases, the effect of the top and bottom oxide film thicknesses on the subthreshold swing decreases. As shown in Fig. 6 and Fig. 7 and (5), the proportional constant K is a function of channel length and channel thickness. Therefore, the subthreshold swing of the asymmetric junctionless DGMOSFET can be calculated by the channel size and the thickness of the top and bottom oxide films.

IV. Conclusions

In this paper, we investigated the relationship between the thickness of the top and bottom oxide films and the subthreshold swing of the asymmetric junctionless DGMOSFET. In contrast to the symmetric structure, the asymmetric structure permits different gate oxide film thickness at the top and bottom sides, and as a result, the short channel effect such as the subthreshold swing can be controlled more effectively. To analyze this, the analytical potential distribution was derived using the Poisson equation and an analytical subthreshold swing model was obtained. We compared the subthreshold swing model proposed in this paper with the two dimensional simulation, and show good agreement for two models. As a result of the analysis of the relationship between the thicknesses of the top and bottom oxide films and the subthreshold swing, it was found that the gate oxide thicknesses at the top and bottom sides must maintain an inversely proportional relationship in order to exhibit a subthreshold swing equivalent to that of the symmetric structure. In addition, in the case of the asymmetric junctionless DGMOSFET, the subthreshold swing is linearly proportional to the geometric mean of the top and bottom gate oxide thicknesses, and the proportional constant is a function of channel length and channel thickness. These results can be used as basic data for the fabrication of junctionless DGMOSFETs with asymmetric structure.

References

[1] V. M. Srivastavaa, K. S. Yadavb, and G. Singh, "Design and performance analysis of double-gate MOSFET over single-gate MOSFET for RF switch," *Microelectronics J.*, vol. 42, no. 3, pp. 527-534, March 2011.

[2] V. Narendar and R. A. Mishra, "Analytical modeling and simulation of multigate FinFET devices and the impact of high-k dielectrics on short channel effects (SCEs)," *Superlattices and Microstructures*, vol. 85, pp. 357-369, Sep. 2015.

[3] V. Kumari, K. Sharmetha, M. Saxena, and M. Gupta, "Underlapped FinFET on insulator: Quasi3D analytical model," *Solid-State Electronics*, vol. 129, pp. 138-149, Mar. 2017.

[4] P. Goutham and S. P. V. M. Rao, "A short channel double gate mosfet model," *Int. Journal of Advanced Research in Electrical, Electronics and Instrumentation Engineering*, vol. 5, pp. 7492-7496, Sep. 2016.

[5] T. K. Sachdeva, S. K. Aggarwal, and A. K. Kushwaha, "Design, analysis & simulation of 30 nm cylindrical gate all around MOSFET," *Int. Journal of Advanced Research in Computer and Communication Engineering*, vol. 5, no. 10, pp. 358-360, Oct. 2016.

[6] N. Trivedi, M. Kumar, S. Haldar, S. Deswal, M. Gupta, and R. S. Gupta, "Analytical modeling of junctionless accumulation mode cylindrical surrounding gate MOSFET (JAM-CSG)," *Int. Journal of Numerical Modeling,* vol. 29, no. 6, pp. 1036-1043, Nov./Dec. 2016.

[7] X. Lin, B. Zhang, Y. Xiao, H. Lou, L. Zhang, and M. Chan, "Analytical current model for long-channel junctionless double-gate MOSFETs," *IEEE Trans. Electron Device.*, vol. 63, no. 3, pp. 959-965, Mar. 2016.

[8] Ajay, R. Narang, M. Saxena, and M. Gupta, "Modeling of gate underlap junctionless double gate MOSFET as bio-sensor," *Materials Science in Semiconductor Processing*, vol. 71, pp. 240-251, Nov. 2017.

[9] F. Jazaeri, N. Makris, A. Saeidi, M. Bucher, and J. Sallese, "Charge-based model for junction FETs," *IEEE Trans. Electron Device.*, vol. 65, no. 7, pp. 2694-2698, Jul. 2018.

[10] A. Cerdeira, M. Estrada, J. Alvarado, I. Garduno, E. Contreras, J. Tinoco, B. Iniguez, V. Kilchytska, and D. Flandre, "Review on double-gate MOSFETs and FinFET modeling," *FACTA UNIVERSITATIS Series: Electronics and Energetics*, vol. 26, no. 3, pp. 197-213, Dec. 2013.

[11] Q. Xie, Z. Wang, and Y. Taur, "Analysis of short-channel effects in junctionless DG MOSFETs," *IEEE Trans. Electron Devices*, vol. 64, no. 8, pp. 3511-3514, Aug. 2017.

[12] A. Nandi, A. K. Saxena, and S. Dasgupta, "Analytical modeling of a double gate MOSFET considering source/drain lateral gaussian doping profile," *IEEE Trans. Electron Device.*, vol. 60, no. 11, pp. 3705-3709, Nov. 2013.

[13] C. Jiang, R. Liang, J. Wang, and J. Xu, "A two-dimensional analytical model for short channel junctionless double-gate MOSFETs," *AIP ADVANCES*, vol. 5, p. 057122, 2015.

[14] Z. Ding, G. Hu, J. Gu, R. Liu, L. Wang, and T. Tang, "An analytic model for channel potential and subthreshold swing of the symmetric and asymmetric double-gate MOSFETs," *Microelectronics J.*, vol. 42, no. 3, pp. 515-519, March 2011.

[15] G. Dhiman and P. K. Ghosh, "Threshold voltage modeling for nanometer scale junction less double gate MOSFET," *Int. Journal of Applied Engineering Research*, vol. 12, no. 9, pp. 1807-1810, 2017.

[16] K. Suzuki, T. Tanaka, Y. Tosaka, H. Horie, and Y. Arimoto, "Scaling theory for double-gate SOI MOSFETs," *IEEE Trans. Electron Devices*, vol. 40, no. 12, pp. 2326-2329, Dec. 1993.

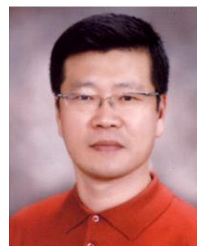

Hakkee Jung received the B.S. degree from Ajou University, Korea, in 1983, the M.S. and Ph.D. degrees from Yonsei University, Seoul, Korea, in 1985, 1990, respectively, all in electronic engineering. In 1990, he joined Kunsan National University, Chonbuk, Korea, where he is currently a Professor in Department of Electronic Engineering. From 1994 to 1995, he held a research position with the Department Electronic Engineering, Osaka University, Osaka, Japan. From 2004 to 2005 and from 2015 to 2016, he was with the School of Microelectronic Engineering, Griffith University, Nathan, QLD, Australia. His research interests include semiconductor device physics and device modeling with a strong emphasis on quantum transport and Monte Carlo simulations. Prof. Jung received the best paper award from The Korean Federation of Science and Technology Societies 2010, and he was the president for Korea Institute of Information and Communication Engineering from 2014 to 2015.

©2019 Int. J. Elec. & Elecn. Eng. & Telcomm.